Article:

Ni, Z, Chu, F, Li, S et al. (2 more authors) (2021) Impact-induced hole growth and liquid film dewetting on superhydrophobic surfaces. Physics of Fluids, 33 (11). 112113. ISSN 1070-6631

https://doi.org/10.1063/5.0073412

Impact-induced hole growth and liquid film dewetting on superhydrophobic surfaces

Zhongyuan Ni (倪中原),[1] Fuqiang Chu (褚福强),[2,a)] Shaokang Li (李少康),[3] Jia Luo (罗佳),[1] and Dongsheng Wen (文东升)[1,4,a)]

[1]*School of Aeronautic Science and Engineering, Beihang University, Beijing 100191, China*

[2]*School of Energy and Environmental Engineering, University of Science and Technology Beijing, Beijing 100083, China*

[3]*School of Engineering, University of Edinburgh, Edinburgh EH9 3FB, United Kingdom*

[4]*School of Chemical and Process Engineering, University of Leeds, Leeds LS2 9JT, United Kingdom*

[a)]*Authors to whom correspondence should be addressed: chu_fuqiang@126.com, d.wen@buaa.edu.cn*

Abstract: Wetting and dewetting phenomena occur widely in the fields of coating, anti-icing, and microfluidics. While liquid wetting via hole collapse has been intensively researched, liquid film dewetting, especially that induced by hole growth, has rarely been studied. This paper describes a combined experimental and theoretical investigation of metastable liquid film dewetting on superhydrophobic surfaces induced by dry hole growth. Experiments show that dry holes can form upon droplet impact, and these holes mainly exhibit growth, stability, or collapse depending on their initial size. Only the growth behavior can induce liquid film dewetting. Theoretical analysis further clarifies that the hole behavior is the result of competition between the capillary force and hydrostatic pressure, and the scale of the dewetting area is controlled by the Young–Laplace equation and affected by the shape of the superhydrophobic surface. The quantitative relationship between the dewetting velocity and the liquid film thickness is also established. These results deepen our understanding of liquid film dewetting on superhydrophobic surfaces and present fresh insights into related engineering applications.

I. INTRODUCTION

Dewetting is the process whereby a liquid film retreats spontaneously from different substance interfaces.[1-6] This phenomenon is ubiquitous in nature, such as in the rapid drying of animal feathers, as well as in industrial processes such as aircraft icing, inkjet printing, microfluidics, and spray cooling.[5, 7-16] In some processes, it is essential to prevent the dewetting phenomenon. For example, in surface coating, the liquid film must remain intact until it has hardened to avoid cracking. In other industrial processes, the dewetting phenomenon may be desirable.[17] For instance, before an aircraft takes off in cold weather, a non-wettable liquid film is sprayed over its body and wings to prevent a continuous water film from forming; otherwise, the water film may freeze and severely degrade the aircraft's performance, potentially resulting in a catastrophic accident.[7]

In recent decades, the dewetting phenomenon has attracted considerable attention. The dewetting process mainly includes the nucleation and growth of dry holes when the liquid film thickness is of the order of the capillary length.[18, 19] Under external interference, such as the local air pressure or evaporation, the local area of the liquid film will become thinner and eventually rupture to form a dry hole.[20-25] That is, a circular contact line between the liquid, gas, and solid substrate is created.[3] In a liquid film, a dry hole is a defect that may grow or collapse, depending on the thickness of the liquid film, the wettability of the substrate, and various competing forces and boundary constraints. From a viewpoint of surface energy, different wetting behaviors can be distinguished by spreading coefficient S=σ_{SG}-σ_{SL}-σ, where σ is the liquid surface tension, σ_{SG} is the solid–gas interfacial tension, and σ_{SL} is the solid–liquid interfacial tension. In a total wetting regime (S > 0) liquid film is always stable, while in a partial wetting regime (S < 0) the liquid film is metastable or unstable and can dewet below a critical film thickness H_c.[9] The critical film thickness H_c=2$l_c^{0.5}$sin(θ/2), where

$l_c=(\sigma/\rho g)^{0.5}$ is the capillary length, in which ρ is the liquid density, and g is the gravitational constant and θ is the surface contact angle. Above H_c, the liquid film is unconditionally stable and any hole formed in it will always collapse.[9, 26, 27]

The behavior of dry holes has received further attention because it is directly related to the final outcome of the liquid film, i.e., wetting or dewetting. Taylor et al.[28] carried out pioneering research in which an air jet was used to create holes in a water film on a hydrophobic paraffin surface, and holes with a wide range of sizes were observed to remain stationary in the water film. Moriarty et al.[29] developed a numerical model based on lubrication theory and studied the stability of holes in which the surface contact angle is less than 90°. Their results showed that the hole could be unstable and either collapse to form a uniform liquid film or grow to reach a stable state. Lv et al.[30] investigated the process of hole collapse in a liquid film on superhydrophobic surfaces (*i.e.*, contact angle > 150°)[31, 32] in a finite domain. Their results demonstrate that the hole can exist stably in the liquid film when the liquid film volume is below a critical value, but when the liquid film volume exceeds this critical value, the hole collapses within a short time. This critical value is the critical volume of the metastable liquid film, which is determined by the container size, surface wettability, and liquid properties. Though numerous studies have explored the collapse and stability of dry holes, the complex nature of dry hole evolution means that the quantitative relationship between the dry hole behavior and the liquid film dewetting has not yet been determined, especially when the liquid film is metastable and located on a superhydrophobic surface.

Thus, in the present work, we generate dry holes in metastable liquid films on superhydrophobic surfaces via a droplet impacting method. The effect of the hole behavior on the final destiny of the liquid film is then quantitatively discussed. Specifically, we first determine the critical volume of the metastable liquid film experimentally and theoretically. Droplet impacting experiments are then carried out to form a dry hole when the liquid film is in the metastable state, and three typical hole behaviors are observed and characterized depending on the initial hole sizes. Finally, we analyze the relation between the hole parameters and the liquid film behavior, and determine the critical hole diameter for liquid film dewetting. The dewetting velocity is also measured under various conditions. We expect that our results will deepen the understanding of the liquid film dewetting phenomenon on superhydrophobic surfaces and have practical and positive impacts on related engineering fields.

II. EXPERIMENTAL METHOD

To investigate the hole growth and liquid film dewetting phenomena on superhydrophobic surfaces, we design two experimental systems. The first is used to investigate the hole collapse process, allowing us to determine the critical volume of the metastable liquid film on superhydrophobic surfaces. The experimental system contains a liquid injection module and a high-speed camera module, as shown in Fig. 1(a). The liquid injection module is composed of a syringe pump, an injector, and a microneedle. The syringe pump steadily pushes liquid into the container through the microneedle at a flow rate of approximately 1 mL/min. The experimental liquid is deionized water with a liquid density ρ of 998 kg/m^3, surface tension σ of 0.0728 N/m, and capillary length l_c of approximately 2.7 mm. The high-speed camera module, which is used to record the whole experimental process at 500 fps, contains a high-speed camera (Photron FASTCAM Mini UX100, Japan), a light source, and a high-performance computer. In these experiments, deionized water is injected into the experimental container via the liquid injection module. The water first wets the surrounding hydrophilic surface and then pushes toward the center of the surface, forming a hole. As the volume of water increases, the hole gradually shrinks until it collapses, indicating a wetting process. The high-speed camera module records the whole experimental process. We analyze the shrinking and collapse of the hole by processing the recorded high-speed videos.

The second experimental system, which is used to conduct experiments in which droplets impact a liquid film, includes a water film container, a droplet production module, and a high-speed camera module, as shown in Fig. 1(b). The water film container enables the water film thickness H to be adjusted from 2.2–4.9 mm. It is controlled by changing the volume of water injected into the container (the diameter of the container used here is constant, i.e., D_{al}=93 mm). The droplet production module is composed of a syringe pump, an injector, and a microneedle, but its function is different from that in the first experimental system. The syringe pump pushes the injector until a water droplet is hanging from the tip of the needle. When the gravity of the water droplet is greater than the surface tension, the water droplet falls naturally. The diameter of the droplet (D_{drop}) is 2.1±0.03 mm, which relates to the size of the needle. The velocity of the droplet (U_0) hitting the water surface is adjusted by changing the distance between the needle tip and the water surface. We use the Weber number to describe the impact velocity of the droplet, $We=\rho U_0^2 D_{\mathrm{drop}}/\sigma$, and vary We from 113–395. The high-speed camera module is used to record the whole experimental process at 1500 fps through the same equipment composition as for the first experiment. In the second experiments, a droplet of diameter 2.1 mm falls from a certain height (20–70 cm) and impacts the surface of the water film. We analyze the hole behavior and dewetting phenomenon by watching the recorded high-speed videos.

The experimental container is the same for both experimental systems. It has a 31-mm-diameter superhydrophobic region in the center (D_{sh}=31 mm), outside of which is hydrophilic aluminum with a contact angle of 73±6°. The fabrication process of the inside superhydrophobic region has three main steps. First, we cover a template on the center of the bottom surface of the cleaned experimental container. The template is designed with a hollow circle. Then, we spray commercial superhydrophobic solutions (mainly composed of SiO_2 nanoparticles, ethyl alcohol, and silicone resin, Changzhou Nanocoatings Co., Ltd., China) on the template covered container surface. Finally, after a drying process at 100°C in an oven, we obtain the experimental surface containing both superhydrophobic region and hydrophilic region. With the help of the template, we can easily control the transition between the superhydrophobic and the hydrophilic region, and the boundary of the two regions is a sharp edge. The inset in Fig. 1(b) shows a low-magnification scanning electron microscopy (SEM) image and the contact angle measurement of the superhydrophobic region. As can be seen, the superhydrophobic region is rather rough with numerous microstructures. The static contact angle is measured to be 165±5° based on multiple parallel measurements using 5-μL water droplets, indicating excellent superhydrophobicity.

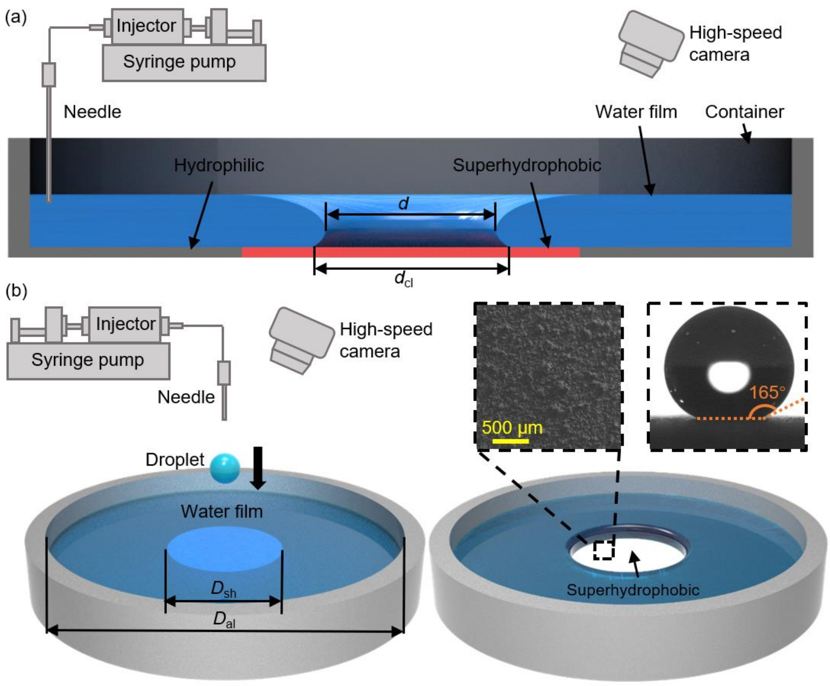

FIG. 1. Schematic of the experimental systems and surfaces. (a) Experimental system for critical volume measurement of metastable liquid film. Water is continuously injected to the container via liquid injection module. d_{cl} is the diameter of the circular line between the liquid, gas, and solid substrate. d is the diameter of the hole, which can be observed from the top view. (b) Experimental system for the droplet impact-induced liquid film dewetting. D_{al} and D_{sh} are the diameters of the container and the superhydrophobic region, respectively. The inset on the right shows an SEM image and contact angle measurements.

III. RESULTS AND DISCUSSION

A. Critical volume of metastable liquid film on superhydrophobic surfaces

The hole collapse experiment, which is a wetting process, allows us to investigate the critical volume of the metastable liquid film. Normally, the liquid film becomes unstable when the thickness is below a critical value H_c in an infinite domain. However, in the container, it is easier for the film to remain stable due to the restriction of the container wall, i.e., the stable thickness in such conditions is $H<H_c$.[30] Therefore, the critical volume is used to define the metastable liquid film in finite domains, and this volume is related to the size of the container, the wettability of the substrate, and the properties of the liquid. The critical volume can be determined by observing the evolution of the hole in the hole collapse experiment. We use the liquid injection module to add water to the container. The hydrophilic region in the container is wetted first, followed by the superhydrophobic region. By continuing to inject water into the container, the circular hole (the experimental image is not absolutely circular since the high-speed camera records with a certain angle of side view) in the superhydrophobic region gradually shrinks, as shown in Fig. 2(a). This is due to the increased hydrostatic pressure as the liquid volume increases, pushing water towards the center of the container. However, if we stop injecting water at any time during this process, the hole will remain static and no longer shrink. We refer to this situation as the hole being stable, i.e., the evolution of the hole in this process is a succession of quasi-static states. When the hole diameter d is reduced to a specific value d_c, however, the hole suddenly collapses within a short time, as shown in Fig. 2(b), even if the water injection is stopped. In this situation, we say that the hole is unstable. Figure 2(c) shows the evolution of the hole diameter during the experiment. We plot the relationship between the instantaneous value of d and time (t-t_0), and define t_0 as the moment at which the

hole disappears (d=0). The blue data points represent the hole in the stable situation, and the red data points represent the hole in the unstable situation. The hole diameter d decreases linearly with time before it reaches the critical value d_c, because the rate of water injection into the container is fixed. However, when the hole diameter d reaches d_c, the slope of the hole diameter gradually increases, i.e., the shrinking velocity increases. This is mainly caused by the instability when the hole collapses, and it is almost independent of the injection rate. The critical value d_c obtained from the experiment is about 14.9 mm. Therefore, the volume of water corresponding to the critical value d_c is the critical volume V_c of the metastable liquid film, which is about 32.2 mL.

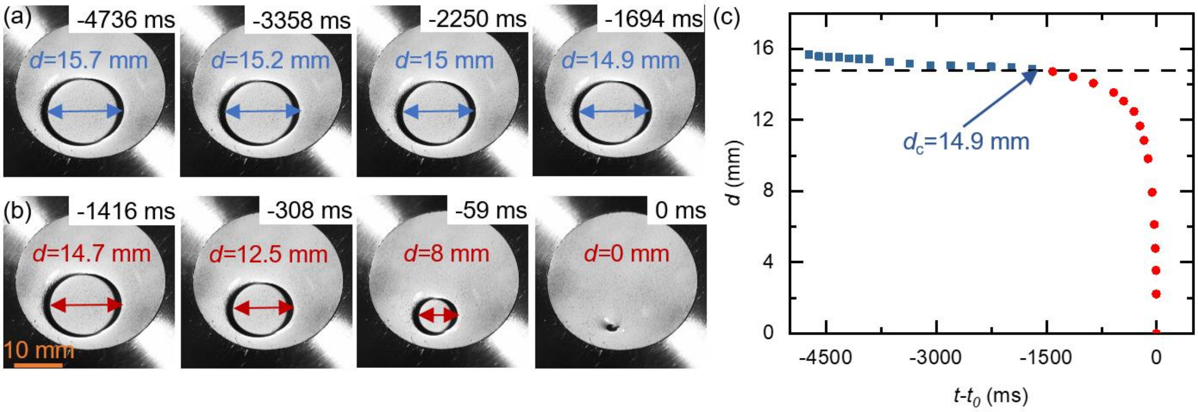

FIG. 2. (a) Top view images of a hole steadily shrinking (D_{al}=93 mm). The white circular region is superhydrophobic. (b) Top view images of a hole collapsing. (c) Time evolution of hole diameter in liquid film. t_0 is defined as the moment at which d=0. The blue data points represent holes in a quasi-steady state. The red data points represent holes in an unstable state. The hole collapses within a short time once the hole diameter is less than d_c.

Next, to understand the underlying mechanisms, we verify the experimental results of the critical volume of metastable liquid film through theoretical analysis. Experiments show that the evolution of the hole is a succession of quasi-static processes before the hole reaches the critical value d_c. The profile of the liquid film can be obtained by the Young–Laplace equation in such conditions. The Young–Laplace equation takes the following dimensionless form in an axisymmetric coordinate system:[29, 30, 33]

$$-\left(\frac{\mathrm{d}\varphi}{\mathrm{d}s^*}+\frac{\sin\varphi}{r^*}\right)\sigma = \Delta p_0^* - z^*, \tag{1}$$

$$\frac{\mathrm{d}r^*}{\mathrm{d}s^*} = \cos\varphi, \tag{2}$$

$$\frac{\mathrm{d}z^*}{\mathrm{d}s^*} = \sin\varphi, \tag{3}$$

where φ is the tangential angle [*i.e.*, φ=arctan(dz/dr)], and $r^*=r/l_c$, $z^*=z/l_c$, $s^*=s/l_c$ [where s is the arc-length along the liquid surface, r is the radial coordinate, and z is the vertical coordinate, as shown in Fig. 3(a)]. Δp_0 is the Laplace pressure at z=0, Δp_0^* is its dimensionless form, $\Delta p_0^*=\Delta p_0 l_c/\sigma$.

The critical diameter d_c is independent of the contact angle for a given container size.[32] Therefore, the critical diameter d_c can be obtained by solving the Young–Laplace equation under the small contact angle condition. If the contact angle is very small (θ<<90°), as shown in Fig. 3(a), the following approximations can be made: $\sin\varphi\approx\varphi\approx \mathrm{d}z^*/\mathrm{d}r^*$ and $\mathrm{d}\varphi/\mathrm{d}s^*\approx \mathrm{d}^2z^*/\mathrm{d}r^{*2}$. Equations (1)–(3) can be rewritten as the following linear second-order ordinary differential equation:

$$\frac{d^2z^*}{dr^{*2}}+\frac{1}{r^*}\frac{\mathrm{d}z^*}{\mathrm{d}r^*}-z^*=-\Delta p_0^*. \tag{4}$$

The boundary conditions are $z^*|_{(r^*=d^*/2)}=0$, $z^{*\prime}|_{(r^*=d^*/2)}=\tan\theta$, $z^{*\prime}|_{(r^*=D^*/2)}=0$, where $d^*=d/l_c$ and $D^*=D_{al}/l_c$. Using these boundary conditions, we can obtain the analytical solution of Eq. (4) and the contour shape of the liquid film profiles. As the analytical solution to this equation cannot be expressed by elementary functions, Bessel functions are adopted to express the solution as:

$$z^*(r^*)=\frac{I_1\left(\frac{D^*}{2}\right)\left[K_0(r^*)-K_0\left(\frac{d^*}{2}\right)\right]+K_1\left(\frac{D^*}{2}\right)\left[I_0(r^*)-I_0\left(\frac{d^*}{2}\right)\right]}{I_1\left(\frac{d^*}{2}\right)K_1\left(\frac{D^*}{2}\right)-I_1\left(\frac{D^*}{2}\right)K_1\left(\frac{d^*}{2}\right)}tan\theta, \tag{5}$$

where I_n is the modified Bessel function of the first kind, K_n is the Bessel function of the second kind, and n is the order of the Bessel function.[29, 34] The analytical solution for the volume V can be deduced as:

$$V^*\left(\frac{d^*}{2}\right)=(\Gamma_1+\Gamma_2)\pi tan\theta, \tag{6}$$

$$\Gamma_1=\frac{\left[\frac{1}{4}(d^{*2}-D^{*2})I_0\left(\frac{d^*}{2}\right)-d^*I_1\left(\frac{d^*}{2}\right)\right]K_1\left(\frac{D^*}{2}\right)}{I_1\left(\frac{d^*}{2}\right)K_1\left(\frac{D^*}{2}\right)-I_1\left(\frac{D^*}{2}\right)K_1\left(\frac{d^*}{2}\right)}, \tag{7}$$

$$\Gamma_2=\frac{\left[\frac{1}{4}(d^{*2}-D^{*2})K_0\left(\frac{d^*}{2}\right)+d^*K_1\left(\frac{d^*}{2}\right)\right]I_1\left(\frac{D^*}{2}\right)}{I_1\left(\frac{d^*}{2}\right)K_1\left(\frac{D^*}{2}\right)-I_1\left(\frac{D^*}{2}\right)K_1\left(\frac{d^*}{2}\right)}, \tag{8}$$

where $V^*=V/l_c^3$. In our experiments, the container diameter D_{al} is 93 mm and the capillary length l_c is approximately 2.7 mm. Therefore, D^* is ~34.4 ($D^*=D_{al}/l_c$). We substitute this value of D^* into Eqs. (6)–(8), and obtain multiple curves of d_{cl}/l_c and V/l_c^3 for contact angles of θ=5°, 15°, 25°, 35°, 45°, and 55°. The results are shown in Fig. 3(b). Each curve has a maximum value in the x-axis direction. This is the critical volume under different conditions, and this value is independent of the contact angle for a given container size. The theoretical calculation gives $d_{cl}/l_c=7$, so $d_{cl}\approx18.9$ mm. Note that d_{cl} is the diameter of the circular contact line between the liquid, gas, and solid substrate, which can be directly observed on hydrophilic surfaces from the top view. However, for superhydrophobic surfaces, this circular contact line is blocked by the curved liquid surface from the top view, as shown in Fig. 1(a). Therefore, the diameter d obtained by the experiments is not equal to d_{cl}. The theoretical value of d can also be obtained by using d_{cl} when the liquid film is located on a superhydrophobic surface. We numerically solve Eqs. (1)–(3) using the Matlab function *ode45* with a value of d_{cl}=18.9 mm and the contact angle of the experimental surfaces (θ=165°). The liquid film profile obtained in this way is shown by the blue curve in Fig. 3(c). This curve has r=9.45 mm at H=0, which is $d_{cl}/2$. This is the radius of the circular contact line. The minimum value of r is 8.1 mm, which is the diameter of the hole that can be directly observed from the top view, d_c=16.2 mm. In other words, the critical diameter of the hole d_c obtained by theoretical calculation is 16.2 mm. The relative deviation of d_c between this theoretical value and the experimental measurement (14.9 mm) is 8%. Furthermore, the theoretical liquid film volume given by integrating the curve is 32 mL, which is very close to the experimental value of 32.2 mL, with a relative error of 0.6%. Thus, the experimental and theoretical results are in good agreement with each other.

Through the above experimental and theoretical work, we have obtained the critical volume of the metastable liquid film of the experimental container. Next, we investigate the behavior of dry holes that is induced by droplets impacting the liquid film when the film is below the critical volume.

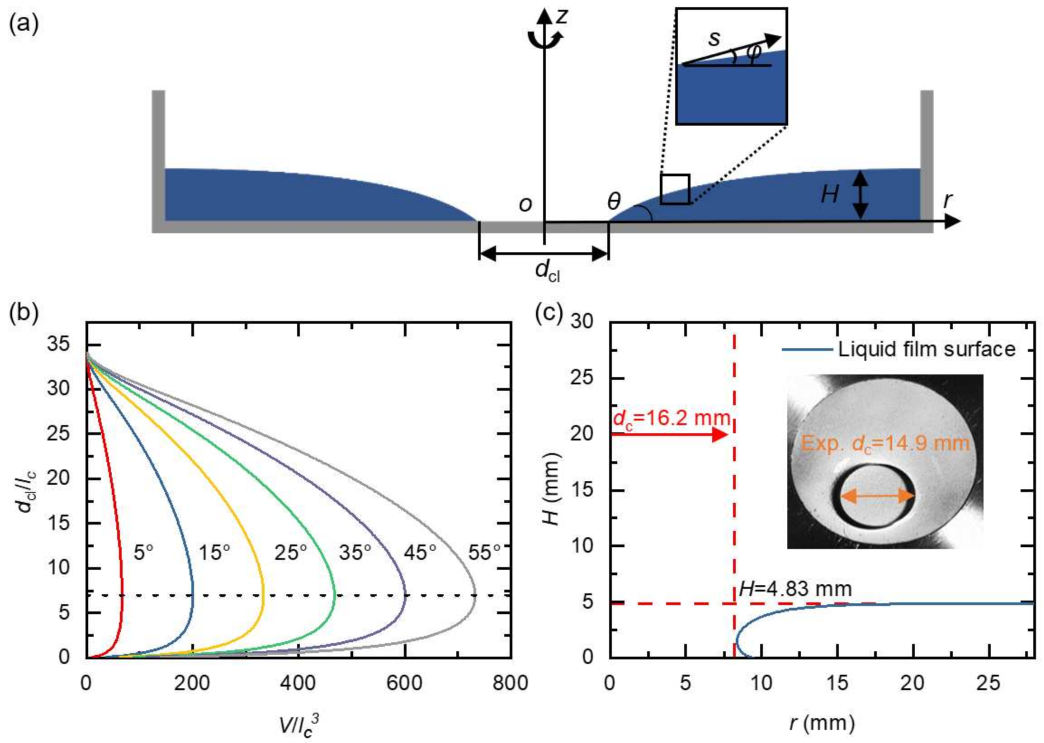

FIG. 3. (a) Schematic of the axisymmetric profile of the liquid film at small contact angle (θ<<90°). (b) Multiple curves of the relationship between liquid volume V and hole diameter d_{cl} given by solving the Young–Laplace equation for small contact angles. Different colors represent different contact angles. The black dotted line represents the hole diameter d corresponding to the maximum volume V of each curve; in each case, $d_{\mathrm{cl}}/l_{\mathrm{c}}$=7. (c) Liquid film profile (blue dots) from numerically solving the Young–Laplace equation for large contact angles (θ>90°). The inset shows the experimental result, which is used as a comparison with the theoretical results.

B. Behavior of dry holes formed by droplets impacting on liquid film

There are many ways to form a dry hole in a liquid film, such as by using an air jet, probe, or droplet impact.[2, 26, 27, 35-37] Here, we use the second experimental system to form dry holes on the liquid film through droplet impact. When a droplet impacts the liquid film, an impact cavity and a crown are initially formed, and these expand so that the residual liquid film at the bottom of the cavity gradually becomes thinner.[38-44] As the superhydrophobic surface is rough, when the residual liquid film becomes very thin, it is affected by the surface microstructure and ruptures.[45] Thereafter, a dry hole is formed inside the cavity. In the early stage of hole formation, the hole shape will be severely affected by evolution of the cavity and the crown, which makes it difficult to analyze hole behavior through static theory. To prevent the crown from influencing the results, the initial hole diameter is defined as the size of the hole after the crown is collapsed. By altering the Weber number of the droplet ($We=\rho U_0^2 D_{\mathrm{drop}}/\sigma$) and the thickness of the liquid film H, numerous holes of different initial diameters are formed. It should be noted that, We reflects the ratio of inertia of the impacting droplet to the surface tension, which mainly affects the process of dry hole formation. In other words, the dry hole will not appear if the inertia of the impacting droplet is too small. While we only concern the hole behavior after the hole formation in this work, and once the dry hole is formed, its behavior (growth or shrink) is no longer controlled by the droplet inertia. According to the experiments, the behavior of these holes is mainly divided into three types, as shown in Fig. 4, which are mainly related to the initial hole diameter.

Because the droplet impact point is located in the superhydrophobic region of the container surface, Fig. 4 only shows images within the superhydrophobic region. Figure 4(a) exhibits the dry hole behavior for

U_0=1.98 m/s and H=2.95 mm. The moment at which the droplet impacts the liquid film is t=0 ms. The initial hole is formed after about 20 ms following a series of processes such as cavity expansion, liquid film rupture, and crown collapse, which are accompanied by capillary waves spreading outward. The initial diameter of the hole is 6.6 mm. As shown in the figure, under this initial hole diameter, the hole grows steadily until it reaches the boundary of the superhydrophobic surface, leading to dewetting of the liquid film. The whole process lasts about 100 ms. The superhydrophobic region remains permanently dewetted thereafter.

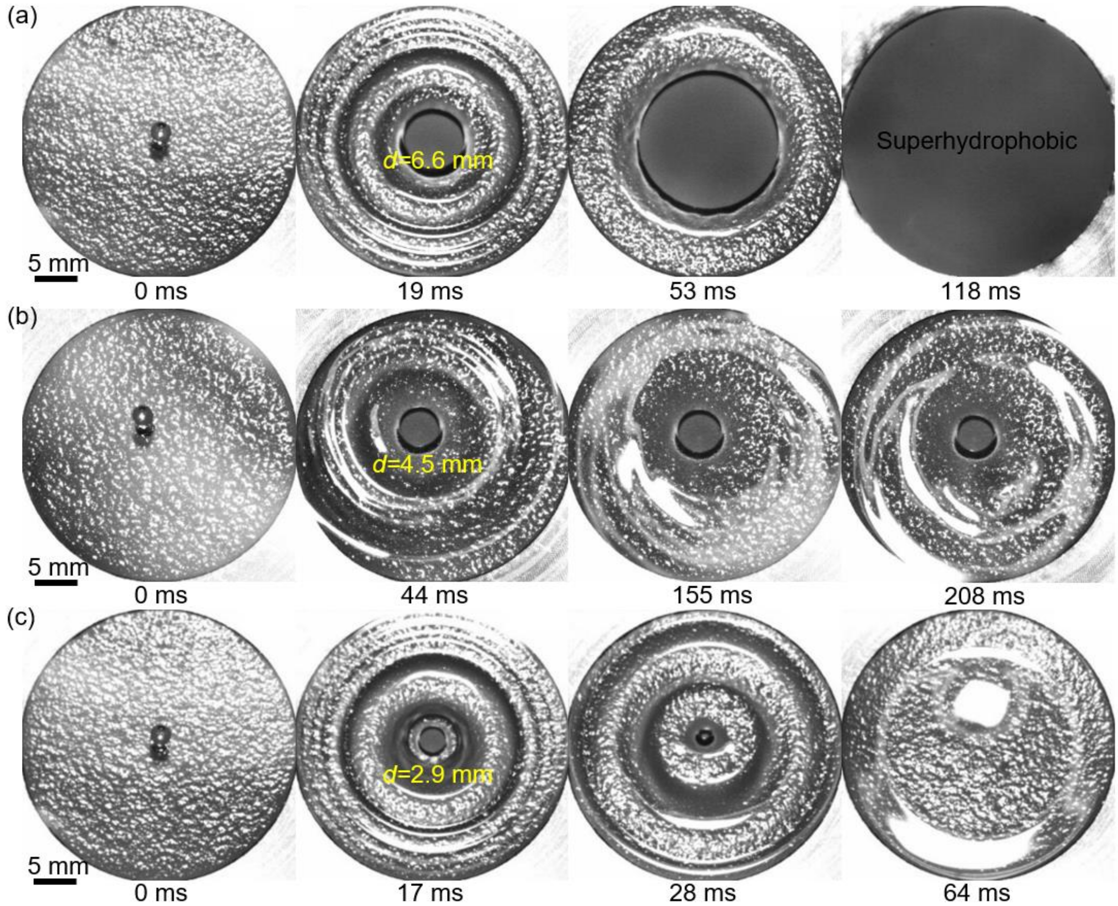

FIG. 4. Top view images of a droplet impacting a liquid film on a superhydrophobic surface. Dark circular areas indicate the superhydrophobic region. (a) Under conditions of U_0=1.98 m/s and H=2.95 mm, the hole formed by droplet impact grows and leads to liquid film dewetting. Multimedia view: (b) Under conditions of U_0=3.13 m/s and H=4.12 mm, the hole remains stable for a long time (~200 ms). Afterwards, the hole disappears under the influence of the capillary wave returning from the container wall. Multimedia view: (c) Under conditions of U_0=1.98 m/s and H=3.54 mm, the hole collapses within a short time (~30 ms). Multimedia view:

Figure 4(b) shows the second kind of dry hole behavior in the case of U_0=3.13 m/s and H=4.12 mm. The hole becomes stable after approximately 44 ms following a complex evolution process. Its initial diameter value is 4.5 mm. After becoming stable, the hole is relatively unchanged until ~200 ms, i.e., it maintains a state of equilibrium. However, this equilibrium is later destroyed by the return of capillary waves from the container walls, which causes the hole to collapse. The liquid film then returns to a calm state. Figure 4(c) shows the third kind of dry hole behavior in the case of of U_0=1.98 m/s and H=3.54 mm. The initial hole (d=2.9 mm) is relatively small after the liquid film ruptures and the crown collapses (~17 ms), and it then collapses within a short time (~30 ms). Similarly, the liquid film returns to a calm state after fluctuating. The whole process lasts about 70 ms. The above experimental phenomena illustrate that the hole behaviors (growth, stability, or collapse) are closely related to the initial hole diameter. In the following section, we quantitatively explain the mechanisms of hole behavior and analyze the relation between the hole behavior and the dewetting phenomenon.

C. Critical hole diameter for liquid film dewetting and the dewetting velocity

Figure 5(a) shows many different initial hole diameters generated by droplet impact for liquid film thicknesses from 3.5–4.5 mm. Cases in which the initial hole continues to grow and causes dewetting of the liquid film are marked in red. This is similar to the process described in Fig. 4(a). If the initial hole eventually collapses, the initial hole data points are marked in black. Most of the non-dewetting data points correspond to the process described in Fig. 4(c). Note that the behavior of a stable hole in Fig. 4(b) is also termed non-dewetting because its final fate is to collapse, but this circumstance is relatively rare. The statistical results for different initial hole diameters indicate that there is a clear boundary between dewetting and non-dewetting. The essence of the different hole behaviors is the competition between the driving force and the resistance to hole growth. On superhydrophobic surfaces, the driving force for the hole growth is mainly controlled by the capillary force $Ca \sim (\sigma/H)d^2$, while the resistance is mainly determined by the hydrostatic pressure $P \sim \rho g H^2 d$. The theoretical boundary between the two behaviors can be obtained using the equilibrium condition $Ca=P$. This result is shown by the blue solid line in Fig. 5(a).

To further investigate the dewetting phenomenon, we numerically solve the Young–Laplace equation in the axisymmetric coordinate system and obtain the theoretical curve of the hole diameter d and liquid volume V at contact angles from 160–170°, as shown by the yellow curve in Fig. 5(b). The vertex of the theoretical curve represents the critical volume V_c and corresponding hole diameter d_c of the metastable liquid film. When the liquid film volume V is less than V_c, two values of the hole diameter exist on the theoretical curve, which means that two specific holes with different diameters can exist stably under this volume. However, the smaller hole is not absolutely stable and will grow to become the larger hole with the same volume on the theoretical curve, or collapse and return to a complete liquid film under some external disturbance. Therefore, we modify the liquid film thickness H of the experimental data in Fig. 5(a) to give the volume V and plot the results in Fig. 5(b). There is a good agreement between the theoretical and experimental results when the liquid film volume is relatively small. As the liquid film volume increases, the experimental data diverge from the theorical values to some extent. Through the above analysis, we can ascertain that small holes may grow to become large holes which theoretically correspond to the same volume. However, the diameter of the superhydrophobic region in this experiment is only 31 mm, and the holes grow to the boundary of the superhydrophobic region and then stop, as shown by the red arrows in Fig. 5(b). This is due to the contact line pinning that occurs on hydrophilic surfaces. Thus, the area of liquid film dewetting can be accurately controlled by designing superhydrophobic surfaces of various shapes.

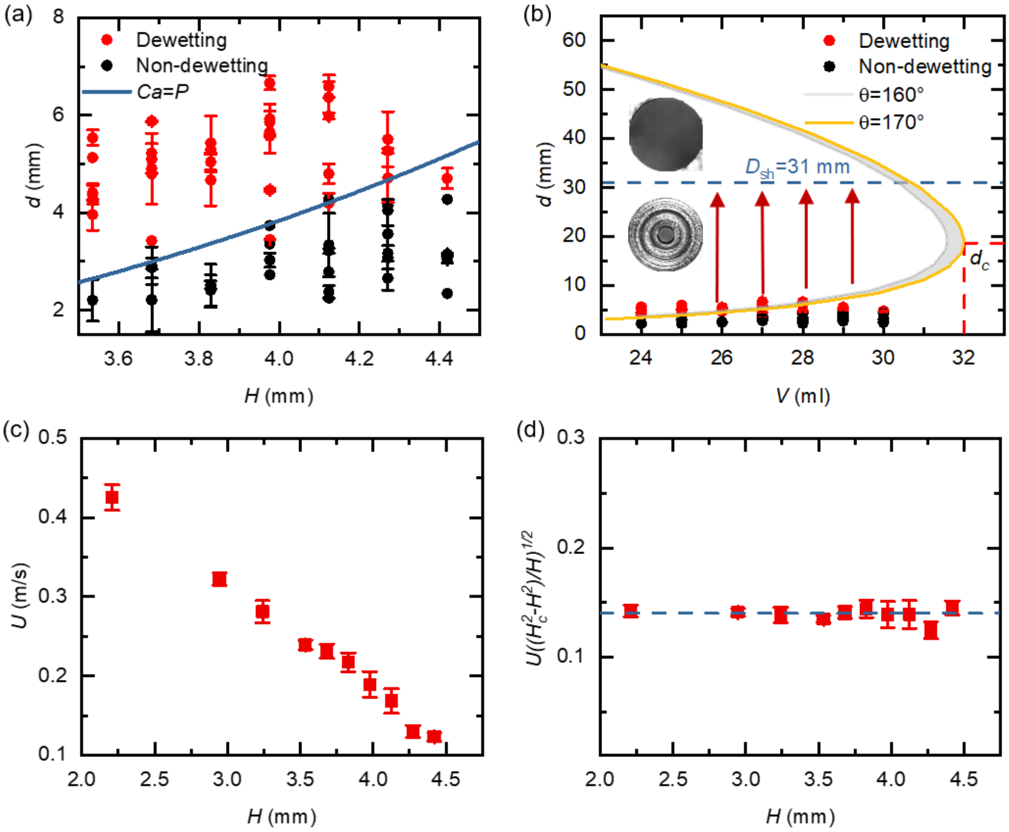

FIG. 5. (a) Initial hole diameter under different liquid film thicknesses. The red and black dots represent dewetting and non-dewetting phenomena, respectively. (b) Theoretical curve of hole diameter d and liquid volume V at a contact angle of 170° (yellow curve in the graph). Shaded area around the curve denotes the theoretical curves at contact angles ranging from 160–170°. In the figure, d_c is the largest critical hole diameter corresponding to the critical volume in this experiment. The blue dotted line represents the diameter of the superhydrophobic region (D_{sh}=31 mm). The red and black data points correspond to the experimental data in Fig. 5(a). The red arrow indicates that holes grow to the boundary of the superhydrophobic region and then stop (insets). (c) Dewetting velocity of liquid film with different liquid film thicknesses. (d) Experimental data in (c) replotted based on Eq. (11). The blue dotted line indicates that the experimental data collapse onto a horizontal line.

Finally, we investigate the growth velocity of the holes, i.e., the dewetting velocity of the liquid film. The experimental results show that the dewetting velocity of the liquid film on superhydrophobic surfaces is approximately constant. Figure 5(c) shows that the dewetting velocity decreases as the liquid film thickness increases. We further analyze the relationship between the dewetting velocity and liquid film thickness using the theory of inertial dewetting. The spreading coefficient is defined as $S=\sigma_{SG}-\sigma_{SL}-\sigma$. During dewetting, S is negative and the corresponding surface energy decreases. The dewetting dynamics of a liquid on a superhydrophobic surface are mainly controlled by the rate of conversion of surface energy to liquid kinetic energy. This process is an inertial dewetting state at Re>>1. According to the theory of inertial dewetting,[7, 26, 27] we have that:

$$\frac{d(MU)}{dt} = F_M - F_v, \tag{9}$$

where M is the mass of the dewetting edge ($M=\rho Hd/2$, where ρ is liquid density, H is liquid film thickness, and d is the diameter of the hole) and U is the dewetting velocity. F_M is the driving force, which is equal to the effective spreading coefficient S^*:

$$S^* = S\left(\frac{H_c^2 - H^2}{H_c}\right), \quad (10)$$

where F_v is friction, which can be neglected on superhydrophobic surfaces. Therefore, the dewetting velocity U can be written as:

$$U \sim \sqrt{\left(\frac{H_c^2 - H^2}{H}\right)}. \quad (11)$$

The experimental data in Fig. 5(c) collapse onto the horizontal line in Fig. 5(d) based on Eq. (11). The above analysis clarifies the quantitative relationship between the dewetting velocity and the liquid film thickness, when the contact angle on the superhydrophobic region is constant. It should be noted that, in Eq. (11), the parameter, $H_c=2l_c^{0.5}\sin(\theta/2)$, is related to the contact angle, which indicates that the dewetting velocity is also affected by the surface wettability.

IV. CONCLUSIONS

In conclusion, we have experimentally and theoretically investigated the formation of a dry hole after a droplet impacts a metastable liquid film on a superhydrophobic surface, and have found that the growth of the hole may lead to dewetting of the liquid film when its diameter exceeds a certain value. The main conclusions from this study are summarized below.

(1) First, we experimentally investigated the critical volume of the metastable liquid film in a finite container. The profile of the liquid film and critical volume were obtained by solving the Young–Laplace equation. Only when the liquid film in the container is in a metastable state can stable holes be formed in the liquid film to trigger the dewetting phenomenon.

(2) Second, the behavior of dry holes induced by droplet impact was investigated for the case where the liquid film is in the metastable state. There are three main types of hole behavior: growth, stability, and collapse. The occurrence of each behavior mainly depends on the initial hole diameter. Only the hole growth behavior leads to liquid film dewetting (the other two behaviors correspond to non-dewetting of the liquid film). The eventual dewetting diameter can be controlled by designing the shape of the superhydrophobic surface.

(3) Finally, the theoretical boundary between the liquid film dewetting and non-dewetting was determined via the equilibrium of the capillary force and hydrostatic pressure. When the capillary force is stronger, the hole grows and dewetting occurs; otherwise, the hole collapses and non-dewetting occurs. The theoretical correlation between the hole diameter and liquid volume, given by solving the Young–Laplace equation, reflects the maximum size of the holes, i.e., the maximum dewetting area. Furthermore, the relationship between the dewetting velocity and the liquid film thickness was clarified.

ACKNOWLEDGMENTS

This work was supported by the Fundamental Research Funds for the Central Universities (Grant No. FRF-BD-20-09A) and the Integrated Projects utilizing the Space Environment on ISS and CSS supported by CMSA and ESA (Grant No. TGMTYY00-RW-03).

DATA AVAILABILITY

The data that support the findings of this study are available from the corresponding author upon reasonable request.

REFERENCES

1. A. M. J. Edwards, R. Ledesma-Aguilar, M. I. Newton, C. V. Brown, and G. McHale, "A viscous switch for liquid-liquid dewetting," Commun. Phys. **3**, 6 (2020).

2. T. Kim, and W. Kim, "Viscous dewetting of metastable liquid films on substrates with microgrooves," J. Colloid Interface Sci. **520**, 11 (2018).

3. L. Wang, X. Wang, and Z.-R. Peng, "Impact of geometric factors of roughness on the dewetting dynamics of a liquid film in the Wenzel state," J. Phys. D: Appl. Phys. **54**, 065305 (2021).

4. M. E. Diaz, and R. L. Cerro, "A general solution of dewetting flow with a moving contact line," Phys. Fluids **33**, 103601 (2021).

5. D. Bonn, J. Eggers, J. Indekeu, J. Meunier, and E. Rolley, "Wetting and spreading," Rev. Mod. Phys. **81**, 739 (2009).

6. A. M. J. Edwards, R. Ledesma-Aguilar, M. I. Newton, C. V. Brown, and G. McHale, "Not spreading in reverse: The dewetting of a liquid film into a single drop," Sci. Adv. **2**, 10 (2016).

7. P. D. Gennes, F. Brochard-Wyart, and D. Quéré, *Capillarity and Wetting Phenomena* (Springer, 2004).

8. R. Abbel, P. Teunissen, J. Michels, and W. A. Groen, "Narrow Conductive Structures with High Aspect Ratios Through Single-Pass Inkjet Printing and Evaporation-Induced Dewetting," Adv. Eng. Mater. **17**, 615 (2015).

9. D. Gentili, G. Foschi, F. Valle, M. Cavallini, and F. Biscarini, "Applications of dewetting in micro and nanotechnology," Chem. Soc. Rev. **41**, 4430 (2012).

10. S. Srinivasan, S. S. Chhatre, J. O. Guardado, K. C. Park, A. R. Parker, M. F. Rubner, G. H. McKinley, and R. E. Cohen, "Quantification of feather structure, wettability and resistance to liquid penetration," J. R. Soc., Interface **11**, 11 (2014).

11. J. Li, N. S. Ha, T. Liu, R. M. van Dam, and C. J. Kim, "Ionic-surfactant-mediated electro-dewetting for digital microfluidics," Nature **572**, 507 (2019).

12. J. Z. Wang, Z. H. Zheng, H. W. Li, W. T. S. Huck, and H. Sirringhaus, "Dewetting of conducting polymer inkjet droplets on patterned surfaces," Nat. Mater. **3**, 171 (2004).

13. P. K. Tyagi, R. Kumar, and P. K. Mondal, "A review of the state-of-the-art nanofluid spray and jet impingement cooling," Phys. Fluids **32**, 121301 (2020).

14. T. Sun, L. Feng, X. Gao, and L. Jiang, "Bioinspired Surfaces with Special Wettability," Acc. Chem. Res. **38**, 644 (2005).

15. S. Chatterjee, J. S. Murallidharan, A. Agrawal, and R. Bhardwaj, "Designing antiviral surfaces to suppress the spread of COVID-19," Phys. Fluids **33**, 052101 (2021).

16. A. M. J. Edwards, R. Ledesma-Aguilar, M. I. Newton, C. V. Brown, and G. McHale, "Electrostatic control of dewetting dynamics," Appl. Phys. Lett. **116**, 253703 (2020).

17. L. O. Kornum, and H. K. Raaschou Nielsen, "Surface defects in drying paint films," Prog. Org. Coat. **8**, 275 (1980).

18. A. Sharma, and E. Ruckenstein, "Dewetting of solids by the formation of holes in macroscopic liquid films," J. Colloid Interface Sci. **133**, 358 (1989).

19. R. V. Craster, and O. K. Matar, "Dynamics and stability of thin liquid films," Rev. Mod. Phys. **81**, 1131 (2009).

20. A. I. Fedorchenko, and J. Hruby, "On formation of dry spots in heated liquid films," Phys. Fluids **33**, 023601 (2021).

21. C.-N. Yu, K. Lazaridis, Y. Wu, E. Voroshilov, M. D. Krivilyov, S. D. Mesarovic, and D. P. Sekulic, "Filling a hole by capillary flow of liquid metal–equilibria and instabilities," Phys. Fluids **33**, 034109 (2021).

22. C. Li, D. Zhao, J. Wen, J. Cheng, and X. Lu, "Evolution of entrained water film thickness and dynamics of Marangoni flow in Marangoni drying," RSC Adv. **8**, 4995 (2018).

23. S. Kim, J. Kim, and H.-Y. Kim, "Dewetting of liquid film via vapour-mediated Marangoni effect," J. Fluid Mech. **872**, 100 (2019).

24. S. Kim, J. Kim, and H.-Y. Kim, "Formation, growth, and saturation of dry holes in thick liquid films under vapor-mediated Marangoni effect," Phys. Fluids **31**, 112105 (2019).

25. N. Mulji, and S. Chandra, "Rupture and dewetting of water films on solid surfaces," J. Colloid Interface Sci. **352**, 194 (2010).

26. X. Noblin, A. Buguin, and F. Brochard-Wyart, "Cascade of shocks in inertial liquid-liquid dewetting," Phys. Rev. Lett. **96**, 156101 (2006).

27. N. Peron, F. Brochard-Wyart, and H. Duval, "Dewetting of low-viscosity films at solid/liquid interfaces," Langmuir **28**, 15844 (2012).

28. G. I. Taylor, and D. H. Michael, "On making holes in a sheet of fluid," J. Fluid Mech. **58**, 625 (1973).

29. J. A. Moriarty, and L. W. Schwartz, "Dynamic Considerations in the Closing and Opening of Holes in Thin Liquid Films," J. Colloid Interface Sci. **161**, 335 (1993).

30. C. Lv, M. Eigenbrod, and S. Hardt, "Stability and collapse of holes in liquid layers," J. Fluid Mech. **855**, 1130 (2018).

31. S. Ding, Z. Hu, L. Dai, X. Zhang, and X. Wu, "Droplet impact dynamics on single-pillar superhydrophobic surfaces," Phys. Fluids **33**, 102108 (2021).

32. B. Liu, and Y. Zhang, "A numerical study on the natural transition locations in the flat-plate boundary layers on superhydrophobic surfaces," Phys. Fluids **32**, 124103 (2020).

33. P. G. López, M. J. Miksis, and S. G. Bankoff, "Stability and evolution of a dry spot," Phys. Fluids **13**, 1601 (2001).

34. B. Ji, Q. Song, and Q. Yao, "Limit for Small Spheres To Float by Dynamic Analysis," Langmuir **34**, 10163 (2018).

35. C. W. J. Berendsen, J. C. H. Zeegers, G. C. F. L. Kruis, M. Riepen, and A. A. Darhuber, "Rupture of Thin Liquid Films Induced by Impinging Air-Jets," Langmuir **28**, 9977 (2012).

36. Z. Zheng, M. A. Fontelos, S. Shin, M. C. Dallaston, D. Tseluiko, S. Kalliadasis, and H. A. Stone, "Healing capillary films," J. Fluid Mech. **838**, 404 (2018).

37. Z. Che, and O. K. Matar, "Impact of Droplets on Liquid Films in the Presence of Surfactant," Langmuir **33**, 12140 (2017).

38. N. E. Ersoy, and M. Eslamian, "Capillary surface wave formation and mixing of miscible liquids during droplet impact onto a liquid film," Phys. Fluids **31**, 012107 (2019).

39. T. Khan, N. E. Ersoy, and M. Eslamian, "Droplet impact on a wavy liquid film under multi-axis lateral vibrations," Exp. Fluids **61**, 173 (2020).

40. Y. Li, Y. Zheng, Z. Lan, W. Xu, and X. Ma, "The evolution of droplet impacting on thin liquid film at superhydrophilic surface," Appl. Phys. Lett. **111**, 231601 (2017).

41. G. Liang, and I. Mudawar, "Review of mass and momentum interactions during drop impact on a liquid film," Int. J. Heat Mass Transfer **101**, 577 (2016).

42. B. Ray, G. Biswas, and A. Sharma, "Regimes during liquid drop impact on a liquid pool," J. Fluid Mech. **768**, 492 (2015).

43. H. Shetabivash, F. Ommi, and G. Heidarinejad, "Numerical analysis of droplet impact onto liquid film," Phys. Fluids **26**, 012102 (2014).

44. N. P. van Hinsberg, M. Budakli, S. Gohler, E. Berberovic, I. V. Roisman, T. Gambaryan-Roisman, C. Tropea,

and P. Stephan, "Dynamics of the cavity and the surface film for impingements of single drops on liquid films of various thicknesses," J. Colloid Interface Sci. **350**, 336 (2010).
45. S. Kim, Z. Wu, E. Esmaili, J. J. Dombroskie, and S. Jung, "How a raindrop gets shattered on biological surfaces," Proc. Natl. Acad. Sci. U. S. A. **117**, 13901 (2020).